

hydrogen-bonded water molecules are located at the intersections of the channels. The  $\mu_4$  squarate has  $C_{4h}$  crystallographic symmetry, whereas the  $\mu_2/\mu_2$  squarate and vanadium dimer have  $D_{2h}$  symmetry. The window of the square channels has dimensions  $\sqrt{2}a/2 \times c = 7.04 \times 7.11 \text{ \AA}$ , which is comparable to the pore size of SAPO-40 zeolite ( $6.7 \times 6.9 \text{ \AA}$ ).<sup>[13]</sup> The water cluster in the *ab* plane is further hydrogen-bonded into a layer, resulting in additional eight-membered rings condensed with themselves and the four-membered rings. It is interesting to note that the O...O separation of 2.88 Å in the water tetramer compares well with the results of vibration-rotation tunneling spectroscopy<sup>[14]</sup> and of ab initio calculations.<sup>[15]</sup>

In summary, the two polymeric structures are composed of similar macrocyclic units constructed from cationic octahedral vanadium dimers and squarate anions, a new building principle for supramolecular architectures and microporous structures. The pore sizes are determined by the coordination modes of the bridging squarates: **2** provides large square channels where cyclic water tetramers are located, whereas **1** has a layer structure with rectangular windows within the layer. These first examples show that there is a great potential for the preparation of topologically unique zeolitic materials in the metal squarate system by hydrothermal methods.

### Experimental Section

**1:** A mixture of  $\text{NH}_4\text{Cl}$  (0.60 mL, 0.5 M),  $\text{V}_2\text{O}_5$  (0.0929 g),  $\text{H}_2\text{C}_4\text{O}_4$  (0.2276 g) ( $\text{V}:\text{H}_2\text{C}_4\text{O}_4$  molar ratio = 1:2), and  $\text{H}_2\text{O}$  (10 mL) was sealed in a Teflon-lined stainless autoclave (volume 23 mL), heated at 180 °C for three days, and cooled to 90 °C at 5 °C h<sup>-1</sup>. The product (yellow green crystals of **1**; yield: 0.1740 g, 88% based on V), was filtered off and washed with deionized water. This compound is stable in air and insoluble in water. Monophasic crystalline material was confirmed by X-ray powder diffraction. Thermogravimetric analysis in air showed one-step weight loss of 54.41% over the temperature range 150–400 °C, which agrees well with the theoretical values of 54.1% assuming that the final decomposition product is  $\text{V}_2\text{O}_5$ . IR(KBr):  $\tilde{\nu} = 3483$  (s, OH), 3145 (br, w,  $\text{H}_2\text{O}$ ), 1621 (s, pendant C=O), 1518 and 1456 (s, C=O and C=C), 1086(m), 1145(m), 861 and 843 cm<sup>-1</sup> (m, V-(OH)-V).

**2:** A mixture of  $\text{NH}_4\text{Cl}$  (0.60 mL, 0.5 M),  $\text{V}_2\text{O}_5$  (0.0904 g),  $\text{H}_2\text{C}_4\text{O}_4$  (0.1143 g) ( $\text{V}:\text{H}_2\text{C}_4\text{O}_4$  molar ratio = 1), and  $\text{H}_2\text{O}$  (10 mL) was sealed in a Teflon-lined stainless autoclave (23 mL), heated at 200 °C for three days, cooled to 150 °C at 5 °C h<sup>-1</sup>, and quenched to room temperature. The product (0.1877 g), which is a mixture of dark purple crystals of **2** and an about equal amount of **1**, was filtered off and washed with deionized water. This compound is stable in air and insoluble in water. The compound retains its structure at 200 °C in air with partial loss of water molecules, and decomposes at 250 °C, as indicated from powder X-ray diffraction and thermogravimetric analysis. IR(KBr):  $\tilde{\nu} = 3463$  (m, OH), 2900 (br, w), 1500 (s, C=C and C=O), 870 cm<sup>-1</sup> (m, V-(OH)-V).

Received: December 23, 1996

Revised version: May 9, 1997 [Z9928IE]

German version: *Angew. Chem.* **1997**, *109*, 2166–2167

**Keywords:** channel structures • hydrothermal syntheses • squarates • supramolecular chemistry • vanadium

- [1] a) C. L. Bowes, G. A. Ozin, *Adv. Mater.* **1996**, *8*, 13–28, and references therein; b) A. Müller, H. Reuter, S. Dillinger, *Angew. Chem.* **1995**, *107*, 2505–2539; *Angew. Chem. Int. Ed. Engl.* **1995**, *34*, 2328–2361, and references therein.
- [2] a) S. Turner, O. Kahn, L. Rabardel, *J. Am. Chem. Soc.* **1996**, *118*, 6428–6432; b) H. O. Stumpf, L. Ouahab, Y. Pei, D. Grandjean, O. Kahn, *Science* **1993**, *261*, 447–449; c) S. Decurtins, H. W. Schmalte, R. Pellaux, R. Huber, P. Fischer, B. Ouladdiaf, *Adv. Mater.* **1996**, *8*, 647–652; d) G. De Munno, M. Julve, G. Viau, F. Lloret, J. Faus, D. Viterbo, *Angew. Chem.* **1996**, *108*, 1931–1934; *Angew. Chem. Int. Ed. Engl.* **1996**, *35*, 1807–1810.
- [3] a) B. F. Hoskins, R. Robson, *J. Am. Chem. Soc.* **1990**, *112*, 1546–1554; b) B. F. Abrahams, B. F. Hoskins, D. M. Michail, R. Robson, *Nature* **1994**, *369*, 727–729.
- [4] M. Fujita, Y. J. Kwon, S. Washizu, K. Ogura, *J. Am. Chem. Soc.* **1994**, *116*, 1151–1152.
- [5] a) P. Losier, M. J. Zaworotko, *Angew. Chem.* **1996**, *108*, 2857–2960; *Angew. Chem. Int. Ed. Engl.* **1996**, *35*, 2779–2781; b) S. Subramanian, M. J. Zaworotko, *ibid.* **1995**, *107*, 2295–2297 and **1995**, *34*, 2127–2128.
- [6] P. J. Stang, D. H. Cao, S. Saito, A. M. Arif, *J. Am. Chem. Soc.* **1995**, *117*, 6273–6283.

- [7] a) Y. Wang, G. D. Stucky, *J. Chem. Soc. Perkin Trans 2* **1974**, 925–928; b) K. J. Lin, M. C. Cheng, Y. Wang, *J. Phys. Chem.* **1994**, *98*, 11685–11693.
- [8] I. L. Karle, D. Ranganathan, V. Haridas, *J. Am. Chem. Soc.* **1996**, *118*, 7128–7133.
- [9] Two-dimensional squarate coordination polymers: C. R. Lii, C. C. Wang, Y. Wang, *Acta Crystallogr. Sect. B* **1996**, *52*, 966–975, and references therein.
- [10] Few examples of discrete bimetal squarates have been reported: a) M. I. Khan, Y. D. Chang, Q. Chen, J. Salta, Y. S. Lee, C. J. O'Connor, J. Zubietta, *Inorg. Chem.* **1994**, *33*, 6340–6350; b) A. Müller, R. Rohlfing, E. Krickemeyer, H. Bögge, *Angew. Chem.* **1993**, *105*, 916–918; *Angew. Chem. Int. Ed. Engl.* **1993**, *32*, 909–911.
- [11] Q. Chen, S. Liu, J. Zubietta, *Angew. Chem.* **1990**, *102*, 100–101; *Angew. Chem. Int. Ed. Engl.* **1990**, *29*, 70–72.
- [12] Diffractometer Enraf-Nonius CAD4,  $\text{MoK}\alpha$  radiation, graphite monochromator,  $\omega/2\theta$  scan, direct methods with NRCVAX [16], refinement on  $F^2$  with SHELXL-93 [17]. Structure of **1**:  $\text{C}_8\text{H}_6\text{O}_{12}\text{V}_2$ , monoclinic, space group  $P2_1/c$  (no. 14);  $a = 7.637(3)$ ,  $b = 8.410(3)$ ,  $c = 9.082(3)$  Å,  $\beta = 97.25(4)^\circ$ ;  $V = 578.7(4)$  Å<sup>3</sup>,  $Z = 2$ ,  $2\theta_{\text{max}} = 55^\circ$ ,  $R_1 = 0.035$ ,  $wR_2(F^2) = 0.077$ ,  $GOF = 0.900$ , residual electron density between  $-0.51$  and  $0.47$  e Å<sup>-3</sup>. Structure for **2**:  $\text{C}_8\text{H}_{10}\text{O}_{14}\text{V}_2$ , tetragonal, space group  $P4/mbm$  (no. 127);  $a = 9.959(1)$ ,  $c = 7.113(2)$  Å;  $V = 705.5(2)$  Å<sup>3</sup>,  $Z = 2$ ,  $2\theta_{\text{max}} = 50^\circ$ ,  $R_1 = 0.032$ ,  $wR_2(F^2) = 0.074$ ,  $GOF = 0.983$ , residual electron density between  $-0.45$  and  $0.32$  e Å<sup>-3</sup>. Further details of the crystal structure investigations may be obtained from the Fachinformationszentrum Karlsruhe, D-76344 Eggenstein-Leopoldshafen (Germany), on quoting the depository numbers CSD-406215 (1) and 406216 (2).
- [13] W. M. Meier, D. H. Olson, *Atlas of Zeolite Structure Types*, 3rd ed., Butterworth-Heinemann, Boston, **1992**.
- [14] J. D. Cruzan, L. B. Braly, K. Liu, M. G. Brown, J. G. Loeser, R. J. Saykally, *Science* **1996**, *271*, 59–62.
- [15] S. S. Xantheas, T. H. Dunning, Jr., *J. Chem. Phys.* **1993**, *99*, 8774–8792.
- [16] E. J. Gabe, Y. Le Page, J.-P. Charland, F. L. Lee, P. S. White, *J. Appl. Cryst.* **1989**, *22*, 384–387.
- [17] G. M. Sheldrick, SHELXL-93, Program for Crystal Structure Refinement, Universität Göttingen, Germany, **1993**.

## Topological Bifurcation Analysis: Electronic Structure of $\text{CH}_5^+$

Dominik Marx\* and Andreas Savin

$\text{CH}_5^+$ , the product of the formal addition of a proton to methane, a stable and rigid molecule, is highly fluxional and elusive. The reason is that the electronic energy penalty to switch from one of the many degenerate eclipsed *e*- $\text{C}_s$  global minima to another one is tiny,<sup>[1–5]</sup> the most recent best estimate being as small as 0.8 kcal mol<sup>-1</sup> to the  $\text{C}_{2v}$  transition state.<sup>[5]</sup> This led to speculations that the hydrogen atoms in  $\text{CH}_5^+$  may easily scramble in the rotational-vibrational ground state as a result of pseudorotational rearrangements.<sup>[3, 6]</sup> This picture was recently confirmed by ab initio quantum simulations in which all the nuclei of  $\text{CH}_5^+$  were treated as quantum particles.<sup>[7]</sup> More importantly, it was demonstrated that a  $\text{H}_2$  unit attached to the apex of a  $\text{CH}_3$  tripod is a characteristic geometric feature of the *quantum* ground state of  $\text{CH}_5^+$ .

A fundamental question which arises is what type of chemical bonding ultimately holds such a highly fluxional molecule together. The *e*- $\text{C}_s$  structure is commonly described as consisting

[\*] Dr. D. Marx  
Max-Planck-Institut für Festkörperforschung  
Heisenbergstrasse 1, D-70569 Stuttgart (Germany)  
Fax: Int. code + (711) 689-1701  
e-mail: marx@pr.mpi-stuttgart.mpg.de

Dr. A. Savin  
Laboratoire de Chimie Théorique (CNRS)  
Université Pierre et Marie Curie  
place Jussieu, F-75252 Paris (France)  
Fax: Int. code + (1) 4427 4117  
e-mail: savin@lct.jussieu.fr

[\*\*] We thank Bernard Silvi and Jürg Hutter for useful discussions.

of three standard two-center, two-electron CH bonds, and one electron-deficient three-center, two-electron bond involving the carbon nucleus and the two hydrogen nuclei that form the  $H_2$  unit.<sup>[8, 9]</sup> To what extent is this picture valid taking into account the floppiness that is present even in the ground state? We will answer this question by a topological analysis of the electron localization function ELF<sup>[10]</sup> of representative configurations sampled from ab initio quantum simulations.<sup>[7]</sup>

Let us now concisely describe some important features of the electron localization function. It can be viewed as a local measure of the Pauli repulsion between electrons in three-dimensional space due to the exclusion principle. It thus allows us to define regions of space that are associated with different electron pairs in a molecule or solid. The definition of ELF  $\eta(\mathbf{r})$  is given by Equations (a)–(d), where the sum in (b) and (d) is over

$$\eta(\mathbf{r}) = \frac{1}{1 + (D/D_h)^2} \quad (\text{a})$$

$$D = \frac{1}{2} \sum_{i=1}^N |\nabla \psi_i|^2 - \frac{1}{8} \frac{|\nabla \rho|^2}{\rho} \quad (\text{b})$$

$$D_h = \frac{3}{10} (3\pi^2)^{2/3} \rho^{5/3} \quad (\text{c})$$

$$\rho = \sum_{i=1}^N |\psi_i|^2 \quad (\text{d})$$

all singly occupied one-electron (spin-) orbitals  $\psi_i(\mathbf{r})$  in an  $N$ -electron system. This function is normalized to the interval between 0 and 1, and is large where the Pauli repulsion is small, that is, where two electrons with antiparallel spin are paired in space. Conversely, it is small in the regions between electron pairs. By locating the electron pairs, ELF makes a direct connection with the chemist's view of the chemical bond, often drawn as a line connecting atoms; this property of ELF is not restricted to the equilibrium structure of a molecule and can even be followed during a chemical reaction. We refer to previous work<sup>[10–13]</sup> for an in depth discussion of the properties of ELF, and in particular to Ref.<sup>[14]</sup> for an interpretation within the framework of density functional theory.

The position where ELF attains a maximum value, the attractor, can be used as an electron pair's signature. To identify a region around a maximum, one can consider all the points in space with  $\eta(\mathbf{r}) \geq f$ , which defines the  $f$ -localization domain;  $f$  is a positive constant smaller than the value of the maximum. This region in space can be visualized by showing the isosurface  $\eta(\mathbf{r}) = f$ . The isosurface surrounds only one attractor when  $f$  is close to the value of the corresponding ELF maximum. For a given value of  $f$ , several closed isosurfaces surrounding different attractors can appear. As the value of  $f$  is lowered, different spatially separated  $f$ -localization domains merge, and closed isosurfaces that contain more than one attractor appear. In other words: there is at least one path which joins different attractors as  $f$  is lowered. Of course, the isosurface encompasses all attractors, that is, all electron pairs, in the  $\eta \rightarrow 0$  limit, whereas all attractors are separated in the opposite limit ( $\eta \rightarrow 1$ ).<sup>[15]</sup>

This behavior can be visualized by a bifurcation diagram, which includes only the maxima of ELF and the saddle points where merging occurs.<sup>[16]</sup> The connectivity of these characteristic points represents the hierarchical merging pattern of the isosurfaces. By focussing on that part of the bifurcation diagram with  $\eta(\mathbf{r}) > f$  one can identify the number of attractors within a particular  $f$ -localization domain, as all maxima within this domain will appear connected. This suggests that a covalent bond is the better defined the larger the difference between the ELF-maximum and the saddle point where the first merging occurs.

The usefulness of these ideas is illustrated by depicting two  $f$ -localization domains with  $\eta(\mathbf{r}) \geq 0.98$  and 0.6 (Figure 1 a–c) for the textbook example, methane; only the chemically relevant valence electrons are included explicitly in the calculations, and the inert core electrons are represented by pseudopotentials. There are clearly four well-separated maxima for  $\eta > 0.71$  (Figure 1 a), which can be assigned to the four CH bonds, whereas all four localization domains coalesce below this bifurcation value  $\eta^* \approx 0.71$  (Figure 1 b, c). This leads to the particularly simple bifurcation diagram displayed in Figure 1 d.

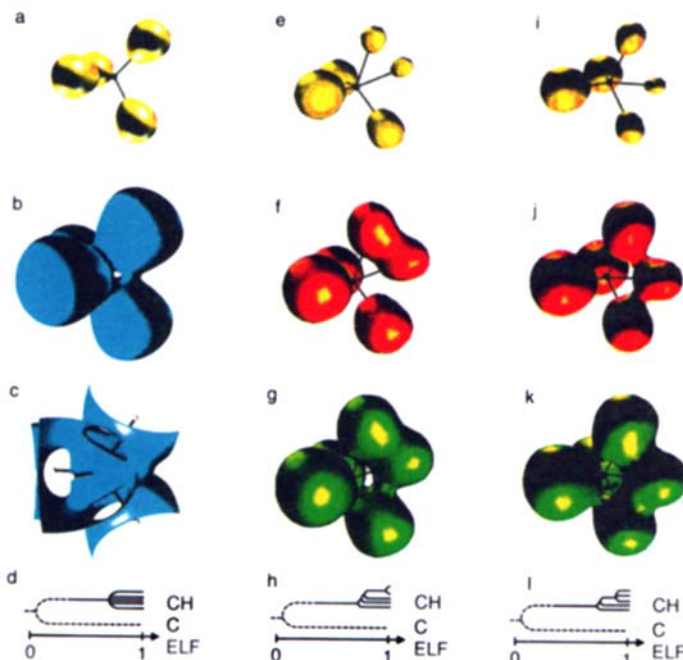


Figure 1. ELF isosurfaces ( $\eta(\mathbf{r}) = f$ ) depicting the  $f$ -localization domains for the global minimum of methane  $CH_4$  with  $f = 0.98$  (yellow, a),  $f = 0.60$  (blue, b), and  $f = 0.60$  with isosurface cut open (blue, c); for protonated methane  $e-C_s-CH_5^+$  with  $f = 0.98$  (yellow, e),  $f = 0.88$  (red, f), and  $f = 0.70$  (green, g); for  $C_{2v}-CH_5^+$  with  $f = 0.98$  (yellow, i),  $f = 0.88$  (red, j), and  $f = 0.70$  (green, k). Resulting valence bifurcation diagrams for methane  $CH_4$  (d), protonated methane  $e-C_s-CH_5^+$  (h), and  $C_{2v}-CH_5^+$  (l). Dotted lines (only schematic): the electrons forming the  $1s^2$  shell of the carbon core are included in the calculations.

Moreover, the attractor structure of ELF allows disjoint spatial regions to be defined from the gradients of ELF.<sup>[12, 17, 18]</sup> From any point in space the gradient is followed to an attractor in that region, and this point is then attributed to this attractor. The collection of all the points in space that were assigned to a given attractor is called its basin. In the example of the valence shell of  $CH_4$ , space is divided into four equivalent basins corresponding to the four CH bonds. Integrating the electron density separately in these valence basins yields 1.98 electrons per basin, very close to two as expected in the idealized Lewis picture of a covalent bond; the last reported digit is assumed to be inaccurate due to the numerical integration on a finite grid. The chemically inert core basin would appear in an all-electron calculation.

The nontrivial case of the quantum-fluxional  $CH_5^+$  can now be approached analogously. First, we have to find the characteristic ELF values at the relevant bifurcation points  $\eta^*$  for the two most important stationary points on the potential energy surface, namely, the  $e-C_s$  global minimum (Figure 1 e–g) and the lowest energy  $C_{2v}$  transition state (Figure 1 i–k). For the global minimum we find five separated maxima for  $\eta \rightarrow 1$ , but two localization domains around them merge already at a surpris-

ingly high value of  $\eta^* \approx 0.97$ . The resulting basin can clearly be associated with the bonding electron pair of the  $H_2$  unit to the carbon nucleus, whereas the other three separated basins stem from the three standard two-center CH bonds in the  $CH_3$  tripod. Integration of the electron density (from the eight valence electrons) over the basins yields values of about two electrons per basin in all four cases (1.72, 1.97, 1.98 for the CH basins, and 2.27 for the  $CH_2$  basin with corresponding CH bonds lengths of about 1.10 Å, 1.08 Å, 1.08 Å, and 1.17 Å, respectively), so one can clearly denote the particular bond that involves two hydrogen nuclei and the carbon nucleus to be a three-center, two-electron bond.<sup>[8,9]</sup> However, these numerical values seem furthermore to suggest that the three-center bond „needs more electrons than just two“ to bind three nuclei, and that the necessary electron density is mainly „borrowed“ from one particular two-center CH bond, which becomes weakened and thus is the longest of the three two-center bonds. This topological pattern is stable over a wide range on the ELF scale down to about  $\eta^* \approx 0.78$ , where the merging of all the valence localization domains starts. The full valence shell is finally established at  $\eta^* \approx 0.7$ ; see Figure 1h for the resulting bifurcation diagram. Thus, we find two distinct bifurcation points  $\eta^*$ : the first where the two isosurfaces surrounding the two hydrogen nuclei of the  $H_2$  unit coalesce and the second where the resulting isosurface now encompassing the  $H_2$  unit merges with the other three isosurfaces stemming from the normal CH bonds.

The bifurcation hierarchy for the  $C_{2v}$  transition state derived from its ELF landscape (Fig. 1i–k) is topologically different (Figure 1l). At  $\eta^* \approx 0.89$  three of the five localization domains merge, and the resulting basin contains four electrons (4.01) that are distributed over four centers (see ref. [5] for such a conjecture), whereas the remaining two basins with about two electrons each (1.97 and 1.96) stem from the two standard two-center, two-electron CH bonds. The full valence shell, that is, the merging of all previously separated basins, occurs at  $\eta^* \approx 0.74$ .

After having determined the characteristic points in the bifurcation hierarchy for the two limiting structures, we can analyze the quantum mechanical ground state of  $CH_5^+$  including tunneling and zero-point motion effects.<sup>[7]</sup> The bifurcation analysis as outlined for the stationary points corresponding to the  $e-C_3$  and  $C_{2v}$  structures is applied to a statistical sample of 64 configurations obtained from previous ab initio quantum simulations.<sup>[7]</sup> We obtain for each of these configurations the ELF from electronic structure calculations based on first principles.<sup>[19]</sup> This gives access to the associated bifurcation diagrams and thus to the ELF values  $\eta^*$  where the two major bifurcations in the valence shell occur in each configuration. The resulting quantity of interest is a histogram or probability distribution  $P(\eta^*)$  of these bifurcation points, and its broadness is entirely due to quantum mechanical tunneling and rotational-vibrational zero-point fluctuations; simulations where the nuclei are approximated as classical particles show that thermal fluctuations are negligible at low temperatures, whereas they are of similar magnitude at room temperature.<sup>[20]</sup>

The two branches of the distribution function depicted separately in Figure 2 show two prominent peaks at the bifurcation points  $\eta^* \approx 0.78$  and 0.97, signaling a major contribution of  $C_3$ -like configurations to the quantum ground state of  $CH_5^+$ . Furthermore, the distribution function actually has minima at  $\eta^* \approx 0.74$  and 0.89, the values that were found to characterize the bifurcation hierarchy of the ideal  $C_{2v}$  structure of  $CH_5^+$ . Thus, the electronic structure analysis based on the bifurcations of ELF clearly supports the concept of a three-center, two-electron bond that holds  $CH_5^+$  together.

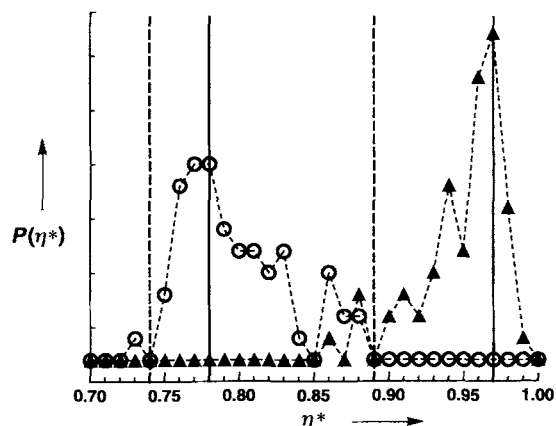


Figure 2. Distribution function  $P(\eta^*)$  of the ELF bifurcation points  $\eta^*$  in the quantum ground state of  $CH_5^+$ ;  $P$  and  $\eta^*$  are dimensionless quantities. The two partial distribution functions obtained from separate histograms of the bifurcation points with the largest (filled triangles) and second largest (open circles) ELF values are shown. The sum of these two contributions constitutes the full distribution function (not shown) and the connecting dotted lines are only visual guides. For the two relevant individual stationary point structures (discussed in the text and presented in Figures 1e–g and i–k) the same analysis yields necessarily very sharp peaks at two ELF values in each case: the vertical solid lines mark these four characteristic peak positions for the  $e-C_3$  global minimum ( $\eta^* \approx 0.78, 0.97$ ), the dashed lines those for the  $C_{2v}$  transition state ( $\eta^* \approx 0.74, 0.89$ ).

In conclusion, we have presented a powerful addition to the arsenal of topological analysis methods of the electronic structure of molecules that is tailored to cope with highly fluxional molecules. In particular, we have demonstrated that a three-center, two-electron bond emerges naturally from this analysis, even for the quantum ground state of such a floppy molecule as protonated methane  $CH_5^+$ . Furthermore, we believe that our method will find widespread applications in the emerging realm of ab initio simulations of molecules at finite temperatures, where one does not deal with a few high-symmetry stationary points, but with an ensemble encompassing many configurations that all deviate from ideal symmetries.

Received: March 3, 1997 [Z 10184 IE]

German version: *Angew. Chem.* 1997, 109, 2168–2170

**Keywords:** ab initio calculations · electron localization · electronic structure · hypervalent compounds

- [1] W. Klopper, W. Kutzelnigg, *J. Phys. Chem.* 1990, 94, 5625–5630.
- [2] P. von R. Schleyer, J. W. d. H. Carneiro, *J. Comput. Chem.* 1992, 13, 997–1003.
- [3] P. R. Schreiner, S.-J. Kim, H. F. Schaefer III, P. von R. Schleyer, *J. Chem. Phys.* 1993, 99, 3716–3720.
- [4] M. Kolbuszewski, P. R. Bunker, *J. Chem. Phys.* 1996, 105, 3649–3653.
- [5] H. Müller, W. Kutzelnigg, J. Noga, W. Klopper, *J. Chem. Phys.* 1997, 106, 1863–1869.
- [6] G. A. Scuseria, *Nature (London)* 1993, 366, 512–513.
- [7] D. Marx, M. Parrinello, *Nature (London)* 1995, 375, 216–218.
- [8] G. A. Olah, *Angew. Chem.* 1995, 107, 1519–1532; *Angew. Chem. Int. Ed. Engl.* 1995, 34, 1393–1405.
- [9] a) G. A. Olah, *Carbocations and Electrophilic Reactions*, VCH, Weinheim, 1974 (see in particular Chapters 3 and 4); b) G. A. Olah, G. K. S. Prakash, J. Sommer, *Superacids*, Wiley, New York, 1985 (see in particular Chapters 3 und 5); c) G. A. Olah, G. K. S. Prakash, R. E. Williams, L. D. Field, K. Wade, *Hypercarbon Chemistry*, Wiley, New York, 1987 (see in particular Chapters 1, 5, and 7).
- [10] A. D. Becke, K. E. Edgecombe, *J. Chem. Phys.* 1990, 92, 5397–5403.
- [11] A. Savin, A. D. Becke, J. Flad, R. Nesper, H. Preuß, H. G. von Schnering, *Angew. Chem.* 1991, 103, 421–424; *Angew. Chem. Int. Ed. Engl.* 1991, 30, 409–412.
- [12] B. Silvi, A. Savin, *Nature (London)* 1994, 371, 683–686.
- [13] R. F. W. Bader, S. Johnson, T.-H. Tang, P. L. A. Popelier, *J. Phys. Chem.* 1996, 100, 15398–15415.

- [14] A. Savin, O. Jepsen, J. Flad, O. K. Andersen, H. Preuß, H. G. von Schnering, *Angew. Chem.* **1992**, *104*, 186–188; *Angew. Chem. Int. Ed. Engl.* **1992**, *31*, 187–188.
- [15] P. Mezey in *Reviews in Computational Chemistry, Vol. 1* (Eds.: K. B. Lipkowitz, D. B. Boyd), VCH, Weinheim, **1990**, pp. 265–294.
- [16] A. Savin, B. Silvi, F. Colonna, *Can. J. Chem.* **1996**, *74*, 1088–1096.
- [17] R. Thom, *Stabilité structurelle et morphogénèse*, Intereditions, Paris, **1972**.
- [18] R. W. F. Bader, *Atoms in Molecules: A Quantum Theory*, Oxford University Press, Oxford, **1990**.
- [19] The Hohenberg–Kohn–Sham density functional formalism in a plane-wave pseudopotential representation is used: R. O. Jones, O. Gunnarsson, *Rev. Mod. Phys.* **1989**, *61*, 689–746. In particular we use the local density approximation supplemented by Becke's exchange gradient correction: J. P. Perdew, A. Zunger, *Phys. Rev. B* **1981**, *23*, 5048–5079 and A. Becke, *Phys. Rev. A* **1988**, *38*, 3098–3100. This method was shown to yield excellent results [7] in particular for the crucial energy difference between the  $e-C_2$  and  $C_2$ , stationary points of  $CH_2^+$  as judged by comparison with correlated high-level calculations [1–5]. Our ELF module is based on the program CPMD version 2.5, written by Jürg Hutter, Max-Planck-Institut für Festkörperforschung, Stuttgart, **1995**, with the help of the group for Numerical Intensive Computations of IBM Research Laboratory Zürich and the Abteilung Parrinello at the Max-Planck-Institut für Festkörperforschung, Stuttgart. Graphics program: E. Pepke, J. Murray, J. Lyons, T.-Z. Hwu, *SciAn*, SCRI, Florida State University, Tallahassee, FL (USA), **1993**.
- [20] D. Marx, M. Parrinello, *Z. Phys. D*, in press.

## Nonclassical Shapes of Noble-Metal Colloids by Synthesis in Microgel Nanoreactors\*\*

Markus Antonietti,\* Franziska Gröhn,  
Jürgen Hartmann, and Lyudmila Bronstein

The controlled synthesis of colloids on a nanometer scale is important for bridging the gap between microlithography and micromechanics, which deal with structures down to 250 nm, and supramolecular chemistry, in which molecules of increasing size are built up by means of sophisticated classical chemistry. Structural design on the intermediate scale of several nanometers requires special techniques; nanomechanics would be inefficient, and classical chemical methods too complex and tedious.

Nature teaches us that effective control of structure is possible. In biomineralization, for instance, functional biomolecules (such as proteins or polysaccharides) act as templates for growing nanocrystals, platelets, and needles.<sup>[1–6]</sup> The specific interaction of these molecules with distinct crystallographic planes or sites of the growing nuclei allows control of the size, shape, and crystal structure of the inorganic product.

This approach for the nanostructuring of materials has been transferred to synthetic chemistry by utilizing Langmuir films of sparingly water soluble organic compounds to direct the growth of calcium carbonate and to tailor its crystal structure and morphology.<sup>[7]</sup> A three-dimensional biomimetic extension was described by Walsh et al., who synthesized highly defined, spongelike inorganic structures by precipitating calcium and magnesium carbonates from the microemulsion phases of non-ionic surfactants.<sup>[8]</sup>

[\*] Prof. Dr. M. Antonietti, F. Gröhn, Dr. J. Hartmann  
Max Planck Institut für Kolloid- und Grenzflächenforschung  
Kantstrasse 55, D-14513 Teltow-Seehof (Germany)  
Fax: Int. code + (3328)46204  
e-mail: pape@mpikg-teltow.mpg.de

Dr. L. Bronstein  
Nesmeyanov Institute of Organoelement Compounds, Moscow (Russia)

[\*\*] Financial support by the Max Planck Society is gratefully acknowledged. L. B. thanks the Volkswagen Foundation for a Russian–German exchange grant. We thank M. Giersig of the Hahn Meitner Institute (Berlin, Germany) for help with high-resolution electron microscopy.

Another route to matter organized on the nanometer scale consists of controlling the intermolecular arrangement of colloids. Fendler and co-workers obtained periodic arrays of noble-metal colloids beneath or in monolayers.<sup>[9]</sup> Möller et al. generated spherical gold particles in block copolymer micelles and examined the surface patterns of drying films.<sup>[10]</sup> Andres et al.<sup>[11]</sup> and Whetten et al.<sup>[12,13]</sup> crystallized gold and silver clusters to give two-dimensional superlattices. All these alignment techniques are restricted to producing crystallike, ordered two-dimensional or three-dimensional arrays of preformed particles, but do not address the original growth process. Nevertheless, these approaches indicate what the further structural layout of nanomaterials may look like.

Currently two general strategies for particle-growth control can be distinguished.<sup>[14]</sup> In host–guest nanoscale synthesis, a cage or structure-directing molecular container is formed by supramolecular or colloidal preorganization in which the nanostructure is fabricated (exo-template approach). In the interfacial molecular recognition route, crystallization is nucleated in the proximity of a structure-directing molecule or assembly. Growth is controlled by the presence of these molecules at some of the crystal surfaces, but no imprinting of an outer shape occurs (endo-template approach).

For a broader application of these principles, simpler, non-biogenic templates are required, and modern polymer chemistry provides some promising candidates. We here describe the use of “microgels”,<sup>[15,16]</sup> spherical polymer gel particles with a well-defined diameter in the nanometer range and an adjustable chemical functionality, as exo-templates and the generation of colloid particles by chemical reactions within the microgels. The tuning parameters of the local chemical environment (cross-linking density, abundance and type of functional groups) and the related physical properties of the microgel (swellability, elasticity) were systematically varied, and the resulting structures of the colloids produced within the nanoreactors investigated.

Using the reduction of gold salts to gold colloids (the classical Faraday experiment) as a model reaction allows a simple evaluation of the experiment by the naked eye. This is because the color of metallic gold colloids is caused by collective oscillations (plasmons) of the electrons relative to the atomic cores, the energy distribution of which is sensitive to the size and shape of the colloidal particles.<sup>[17]</sup>

Figure 1 shows a selection of gold colloids in polystyrene sulfonate microgels. Variation of cross-linking density, reducing agent, and reducing conditions resulted in a variety of stable colloidal solutions with very different colors. In addition to the classical Faraday colors, Barolo red and purple, shades from bengal rose to apricot and black were obtained.

These colloids were characterized by transmission electron microscopy (TEM). Three typical morphologies obtained by varying the reduction conditions are shown in Figure 2. Fast reduction with  $NaBH_4$  in water resulted in the limiting case of small spherical gold colloids located as swarms inside the microgels (Figure 2a). Decreasing the reduction rate by changing the pH ( $NaBH_4$  in 0.1N NaOH), but maintaining all other parameters, led to a second morphology: long and winding gold threads (Figure 2b). With hydrazine as a reducing agent, gold “nanonuggets” that resemble algae were formed (Figure 2c).

The estimated amount of gold in a thread or a nugget is one order of magnitude too large to have originated from the gold load of a single microgel. Dynamic light scattering before and after reduction indicated that the reaction occurred only in some of the dispersed particles, which led to a bimodal particle size distribution. That is, the colloids were nucleated in some of the microgels, while the others served as a source of gold salt which